

# Analysis of the Influence of the Working Angles on the Tool Wear in Gear Hobbing

Felix Kühn, Christoph Löpenhaus and Fritz Klocke

Gear hobbing is one of the most productive manufacturing processes for cylindrical gears. The macro geometry of the cutting edge of a hob is decisively designed on the tool angle. The tool angles are defined as rake angle, wedge angle and clearance angle. In the process, the tool angles change to the working angles as a result of the resulting velocity. The goal of this report is to calculate and optimize the working angles at the hob. First, the tool angles and the working angles along the cutting edge at the hob are explained in detail. A calculation method is developed with the support of the production simulation *SPARTApro*. As the free choice of tool angles is especially possible for hobs with indexable inserts, the simulation of indexable inserts in gear hobbing is presented, as well. The method can be used to calculate the working angles in the hobbing process. Subsequently, the calculation method is applied, a simulation plan is set up, and the working angles are calculated for all variants. With the aid of the calculated working angles, an estimation of the tool wear can be given.

## Introduction and Motivation

One of the most productive processes for the manufacturing of external gears is gear hobbing (Refs. 1–4). The simplest design of a hob is the conventional hob, where the body is made from a single piece of cutting material. The shape of a conventional hob is defined by two categories: macro and micro geometry (Ref. 3). Parameters such as external diameter, tool length, chip flanks, chip gashes and the tool angles belong to the macro geometry category. The tool angles are defined as rake angle, wedge angle and clearance angle.

Until today, there are few scientific investigations regarding the free modification of the tool angles in the gear hobbing process. Only Joppa (Ref. 5) investigated the influence of rake and clearance angles on tool wear in 1977 (Fig. 1; Ref. 5). He varied the angles for HSS-tools in wet processing. As the results show, the tool angles have a significant influence on the wear behavior and the life time of the hob. Since (Ref. 5), coatings and alternative cutting materials such as cemented carbide tools have changed the wear behavior of hobs. In the field of bevel gears, several studies

have shown that specific modifications in the tool angles can lead to an extension in tool life of cemented carbide tools (Refs. 6–7). This potential is also expected for gear hobs. However, the transfer of the research results from bevel gear to spur gears is not directly possible. This is due to the fundamental differences of kinematics between both processes. In gear hobbing each tooth experiences a load spectrum resulting from the different tool positions, the same does not occur in bevel gear plunging. Due to the indicated potential shown by manufacturing of bevel gears, a specific

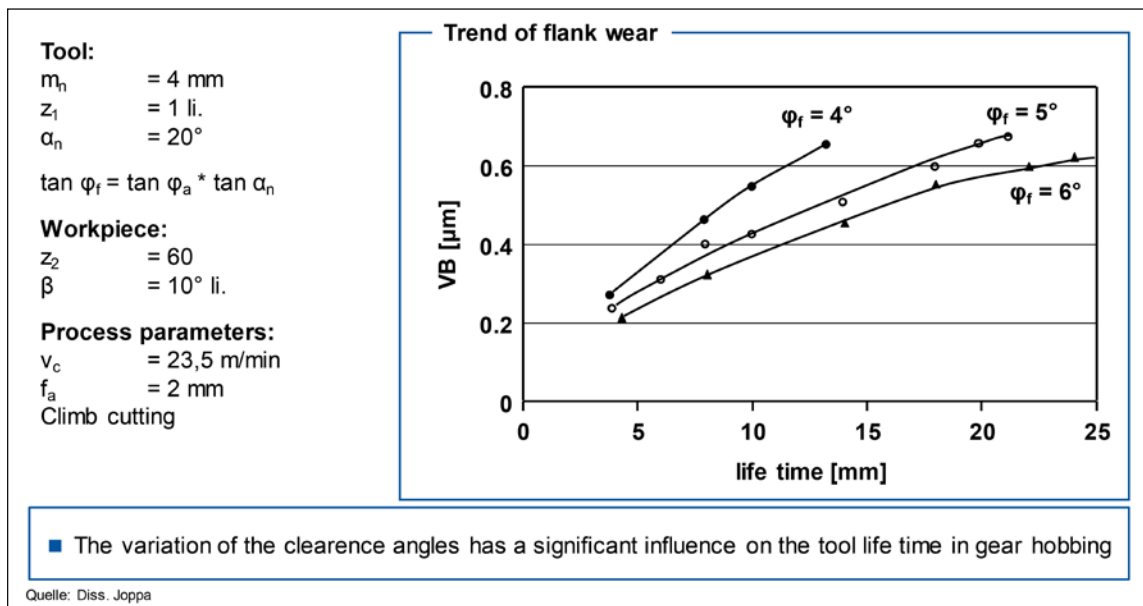


Figure 1 Varied clearance angle (Ref. 5).

modification in the tool angles for the hobbing process is promising. Thus, this report will analyze the influence of the tool angles in gear hobbing process.

## Objective and Approach

In the hobbing process, critical wear can occur on the tool due to the resulting load spectrum at the cutting edge. Basic investigations must be conducted in order to explain basic causes of tool wear and make correlations to specific variables.

The objective of this report is to analyze the hob macro geometry regarding the working angles (Fig. 2). The basis for this is a geometrical penetration calculation taking the clearance

and rake angles during machining into account. For this purpose, the method of penetration calculation developed at WZL, which is integrated in the software *SPARTApro*, will be further developed in order to enable the calculation of working angles during the entire machining process. In addition, the penetration calculation for application of indexable insert has to be developed because the tool angles can be varied by application of indexable inserts. The originality of the work lies in the complete consideration of the influence of the defined tool angles as well as the working tool angles, set during the process, on the tool wear behavior. Previous wear tests of hobbing

processes proved the significant influence of the working clearance and rake angles at the tool cutting edge (Ref. 5). These changes, however, are not only caused by kinematics, but also a function of the generating position. In order to provide a complete understanding of the process and a scientifically and comprehensible analysis of the machining process, the knowledge of the effects of these angles on tool wear is imperative. The scientific contribution of this research is the fundamental investigation of the cutting mechanisms and their effect on the wear behavior. Based on the results obtained, the objective is to achieve an improvement in the machining conditions by

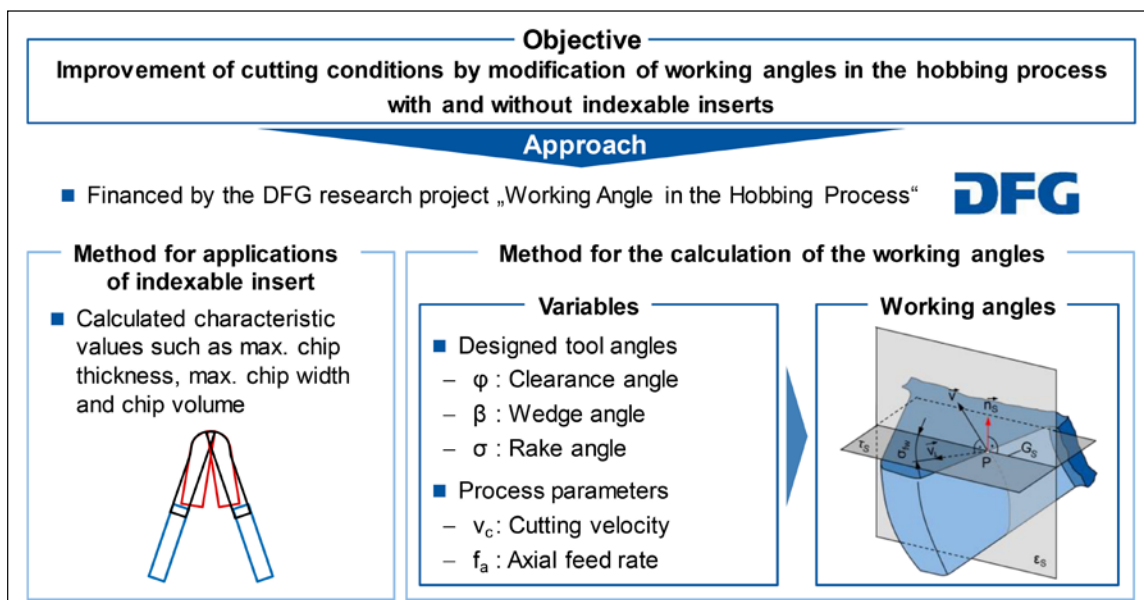


Figure 2 Objective and approach.

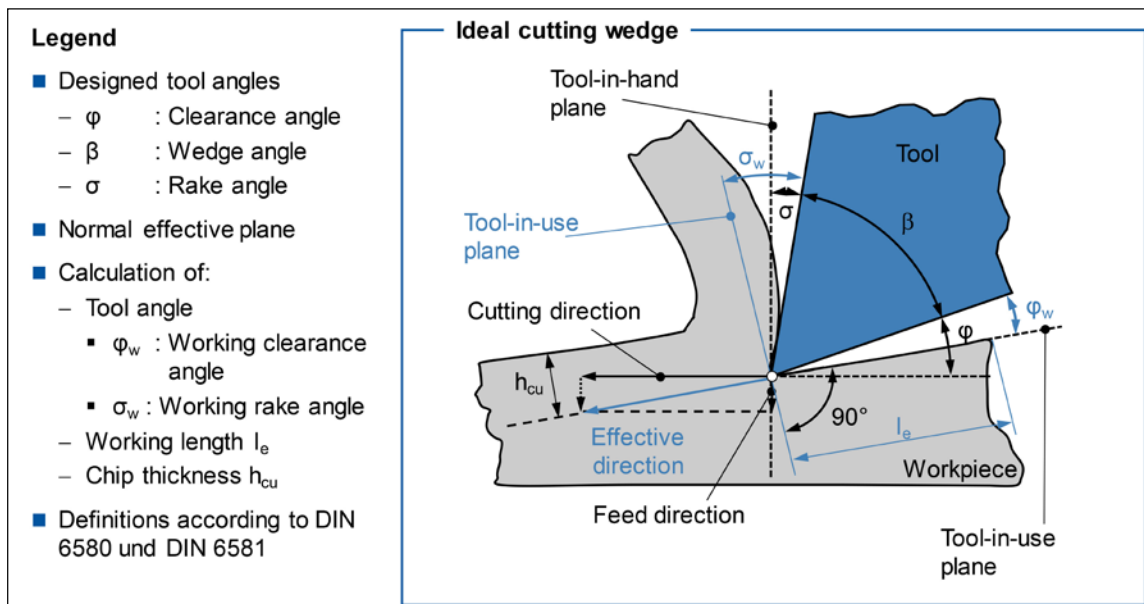


Figure 3 Process kinematics at the idealized cutting wedge.

modifying the working tool angles in the hobbing process.

### Process Kinematics at the Idealized Cutting Wedge

Definitions, nomenclatures and descriptions for the geometry of a tool cutting wedge are specified in the DIN 6581 (Ref. 8). The ideal cutting wedge is represented in Figure 3, which is composed of tool clearance angle  $\varphi$ , wedge angle  $\beta$  and rake angle  $\sigma$ . The correlation between the clearance, tool and rake angles is described in Equation 1.

$$\varphi + \beta + \sigma = 90^\circ \quad (1)$$

- $\varphi$  [°] Clearance angle
- $\sigma$  [°] Rake Angle
- $\beta$  [°] Wedge angle

The clearance angle influences crucially the heat input into the tool. The larger the clearance angle, the smaller is the wedge angle, which leads to a reduction of the tool tip's stability. If the clearance angle is too large, the input of heat can be too great, increasing the tool temperature and leading to a disturbance or loss of the tool hardness (Ref. 9). A small clearance angle improves the heat transfer through the tool. However, if the angle is too small, the contact between the tool clearance surface and the workpiece surface increases. The friction from this contact leads to abrasive wear with negative effect on the tool life (Refs. 6–7).

The rake angle influences the material

forming, which occurs during the cutting process (Ref. 6). The larger the rake angle, the smaller is the chip deformation during cutting. On the other hand, the increase of the rake angle reduces the tool stability. The smaller the rake angle, the larger is the chip deformation. In this case, the chip experiences a larger curvature than usual. It is for this reason that the rake angle influences the resulting cutting forces as well as the temperature along the cutting edge and the rake surface (Ref. 7).

In order to have a clear description of location, position and movement direction of a cutting wedge, a reference system is used, where characteristic planes are defined and applied to all process variants. The two reference systems used are the tool-in-hand system and the tool-in-use system. The tool-in-hand system is used for tool design, as well as for the manufacturing and testing of cutting tools. In this system, the tool angles are measured without considering the process kinematics. During the machining process, the working clearance and rake angles may differ from the designed angles due to the process kinematics. The tool angle remains unmodified. For this reason, the tool-in-use system was created (Ref. 9).

Figure 3 presents the tool-in-use system defined by the effective velocity, which is the result of the vectorial summation of the cutting velocity and the feed rate

velocity. The working clearance angle  $\varphi_w$  calculated in the tool-in-use system is smaller than the tool clearance angle  $\varphi$ . The wedge angle  $\beta$  remains unmodified. Since the relationship stipulated (Eq. 1) is also valid for the tool-in-use system, the variation between the designed rake angle  $\sigma$  and the working rake angle  $\sigma_w$  is the same amount as the variation of the clearance angle—but in a positive direction. In this case, the working rake angle  $\sigma_w$  is larger than the designed rake angle  $\sigma$ .

### Tool Angles in Gear Hobbing in the Tool-In-Hand System

The magnitude of the tool angles of a hob has a direct influence on the chip formation, the cutting force and the tool wear. Partly they have a connection to vibrations and chattering during the process (Ref. 1). For the hob, the designed angles follow the same rules described in the ideal cutting wedge regarding clearance, wedge and rake angles. The designed tool angles are altered along the cutting edge of the hob. This leads to a distinction between the designed angles in the tip and flank of the tool (Fig. 4), which are described with the symbols  $\varphi_a$  for designed tip clearance angle and  $\varphi_f$  for designed flank clearance angle. The designed clearance angle for a specific point  $P$  of the cutting edge is defined as the angle between the plane tangential to the hob clearance surface and the plane tangential to the hob thread, in the same

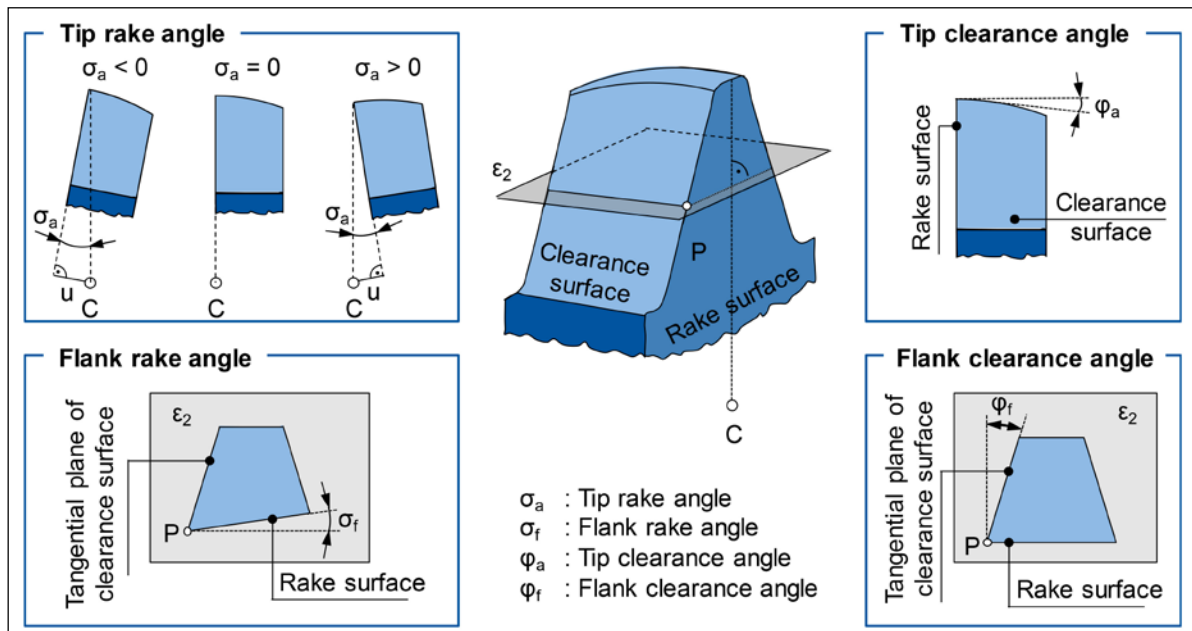


Figure 4 Process kinematics at the idealized cutting edge.

point  $P$  (Ref. 1).

The designed clearance angle is manufactured along the tool cutting edge in circumferential direction according to a logarithmic spiral (Refs. 1, 10). As a result, the designed clearance angle is manufactured. In the case of a conventional hob, there is a relation between the tip clearance angle  $\varphi_a$  and the flank clearance angle  $\varphi_f$ , stated by Equation 2:

$$\tan \varphi_f = \tan \varphi_a \cdot \tan \alpha_0 \quad (2)$$

$\varphi_f$  [°] Flank clearance angle

$\varphi_a$  [°] Clearance angle

$\alpha_0$  [°] Clearance angle

Equation 2 contains the tool profile angle  $\alpha_0$  (Ref. 11). This relation must exist in order to avoid that a re-grinding process in tool modifies the clearance angle along the tool flank as well as the tool profile (Ref. 12). The state of the art for hobs defines tip clearance angle values between  $8^\circ \leq \varphi_a \leq 12^\circ$ , and in special occasions the value can vary between  $12^\circ \leq \varphi_a \leq 20^\circ$ . In case of indexable inserts that are changed after reaching the wear criterion this dependency can be neglected. The geometry of different inserts along the profile can be chosen independently.

For designed rake angles there is also a distinction between the designed tip rake angle  $\sigma_a$  and the designed flank rake angle  $\sigma_f$ . The designed rake angle for a specific point  $P$  localized on the cutting edge is defined as the angle between the plane tangential to the hob

rake surface and the plane through point  $P$  which contains the hob axis (Ref. 1). The rake angle is positive when the plane containing the hob axis touches the cutting wedge in  $P$ . The angle is negative when the plane intersects the cutting wedge.

The designed flank rake angle can be realized by modifying the tool gash angle. For the case of tools gashed parallel to the hob axis (gash angle of  $\gamma_N = 0^\circ$ ), the designed flank rake angle is  $\sigma_f = 0^\circ$ . If the gash angle is  $\gamma_N > 0^\circ$ , a negative flank rake angle  $\sigma_f$  on the right cutting edge is obtained while a positive flank rake angle is obtained on the opposite edge. If  $\gamma_N < 0^\circ$ , the sign of the angles would be inverse.

$$\varphi_a = \arctan\left(\frac{2 \cdot u}{d_a}\right) \quad (3)$$

$\sigma_a$  [°] Tip rake angle

$d_a$  [mm] Tool external diameter

$u$  [mm] Rake surface offset

The designed tip rake angle can be obtained by a face offset "u" in the rake surface position. If the rake surface offset is shifted toward its original position with respect to the hob axis, the tip rake angle  $\sigma_a$  is positive. If the offset is performed in the opposite direction, the tip rake angle is negative. From the amount of offset of the rake surface, the tip rake angle is determined, according to Equation 3.

**Working clearance angle at the hob in the tool-in-use system.** Due to the

resulting velocity on the hob blade in the cutting process, the working clearance angle differs from the designed clearance angle. This modified clearance angle is referred to as working clearance angle  $\varphi_{fW}$ . The direction and magnitude of the difference between designed and working clearance angle is particularly interesting on the flank cutting edges. The clearance angles in the flank cutting edges are smaller compared to the angle in the tip cutting edge. Under inconvenient circumstances, the working clearance angle at the flank edges can reach values close to below  $0^\circ$ . The definition of the working flank clearance angle  $\varphi_{fW}$  is shown (Fig. 5). The center of Figure 5 highlights one tooth of a hob. A random point  $P$  on the cutting edge of the tooth is selected. From the point  $P$ , a normal vector  $n_F$  is drawn, perpendicular to the tangential surface  $\tau_F$  of the flank surface. The vector  $V$  represents the velocity in the point  $P$ , combining three velocity components  $V_{r0}$ ,  $V_{r2}$  and  $V_S$  (Eq. 4). The velocity component  $V_{r0}$  represents the tool rotation around the hob axis, while  $V_{r2}$  represents the component for the workpiece rotation. The third component  $V_S$  represents the feed motion of the hob relative to the workpiece. The individual components of velocity  $V$  take different positions from each other for different angular positions of the hob. This causes the resultant vector  $V$  to change its position with respect to the hob according to the angular position of

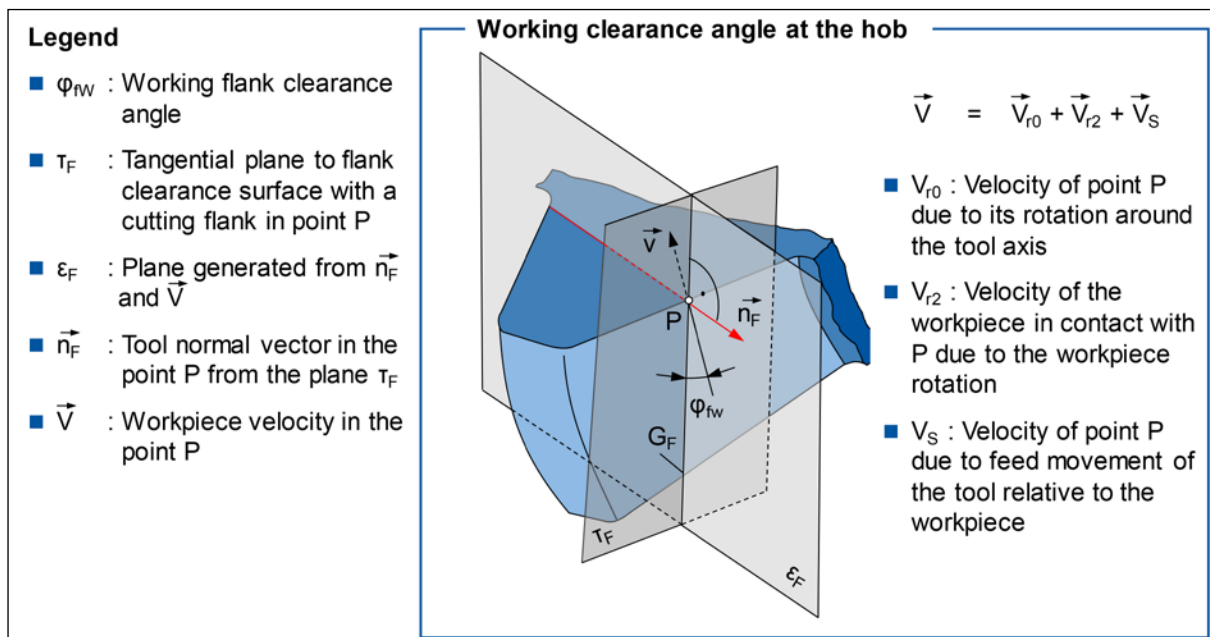


Figure 5 Working clearance angle in gear hobbing.

this same hob.

$$\vec{V} = \vec{V}_{r0} + \vec{V}_{r2} + \vec{V}_s \quad (4)$$

- $\vec{V}$  [m/s] Relative velocity
- $\vec{V}_{r2}$  [m/s] Velocity component resulting from work piece rotation
- $\vec{V}_{r0}$  [m/s] Velocity component resulting from rotation around the hob axis
- $\vec{V}_s$  [m/s] Velocity component resulting from tool feed motion

The vectors  $V$  and  $n_F$  build the plane  $\epsilon_F$ . The intersecting line between the planes  $\epsilon_F$  and  $\tau_F$  is called  $G_F$ . The working clearance angle  $\phi_{fW}$  in the point  $P$  is defined as the angle between vector  $V$  from the relative velocity and the intersecting line  $G_F$ . The working flank clearance angle depends on the process operating

conditions. The velocity component  $V_{r0}$  depends on the distance to the hob axis, which means that  $V_{r0}$  changes for different points on the tool cutting edge.

**Working rake angle at the hob in the tool-in-use system.** The working rake angle  $\sigma$  of a tool mainly depends on two factors: 1) the designed angles and 2) the relative velocity in the considered point. Figure 6 shows a single blade of the hob, where the working rake angle is illustrated. The working rake angle is not constant along the cutting edge. The relative velocity changes through the different velocity components along the cutting edge, as shown Eq. (4). Figure 6 examines point  $P$  in more detail. The velocity in point  $P$

is indicated by the vector  $V$ , and  $\tau_s$  is the plane tangential to the rake surface. The normal vector  $n_s$  is perpendicular to the tangential plane  $\tau_s$ . The velocity  $V$  and the normal vector  $n_s$  build the plane  $\epsilon_s$ . Vector  $V^*$  has the same module of vector  $V$ , but it is rotated by  $90^\circ$  to the vector  $V$  in the plane  $\epsilon_s$ . The plane  $\epsilon_s$  is perpendicular to plane  $\tau_s$ , and the intersecting line between both planes is called  $G_s$ . The working flank rake angle  $\sigma_{fw}$  is measured between the vector  $V^*$  and the cutting line  $G_s$ .

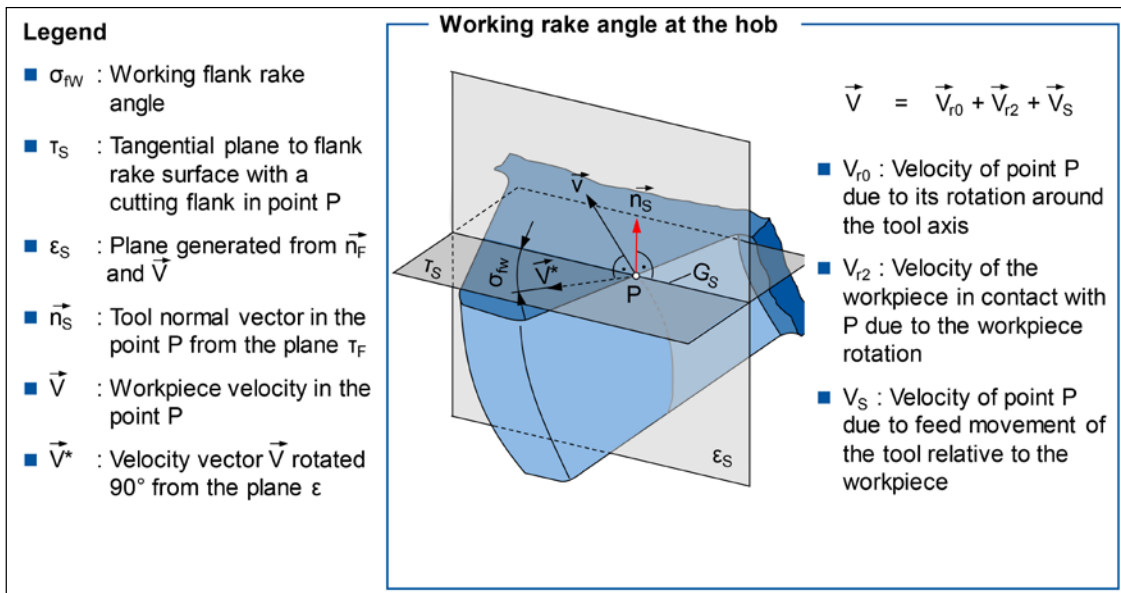


Figure 6 Working rake angle in gear hobbing.



Figure 7 Manufacturing simulation software SPARTApro.

## Further Development of the Penetration Calculation SPARTApro

The Laboratory for Machine Tools and Production Engineering in Aachen (WZL) developed specific software to simulate the process of gear hobbing, i.e. — SPARTApro (Fig. 7; Refs. 13–15). Based on the input information regarding tool geometry, workpiece geometry and process parameters the tooth gap is generated with the assistance of a numerical penetration calculation. During simulation, the final chip geometry is determined. With the chip geometry characteristic values such as maximum chip thickness  $h_{cu,max}$ , maximum chip length  $l_{max}$  and machined volume  $V$  can be calculated. These characteristic values are important for the determination of mechanical and thermal loads at the cutting edge of the tool.

**Applications of indexable inserts.** The difference between indexable insert tools and conventional tools exists in the division of the tool profile into different cutting sections. Each cutting section consists of one indexable insert; the number of cutting sections increases according to the module of the tool. For small-module hobs the profile is divided into two sections — each with one indexable insert. One indexable insert cuts the left side of the gap and one indexable insert cuts the right side of the gap. For large-module hobs the profile is divided

into more than two sections. Especially the tip area of the tool can consist of several indexable inserts as this area shows the maximum chip thickness that can be reduced by an overlap.

In addition to the distribution of the profile, the cutting sections are also distributed along the tool circumference in order to create cutting edges for all hob gashes. In most cases, the angles between the individual cutting sections are constant. This results in equal loads for all indexable inserts. But also changing angles between the cutting sections are used to distribute the load on different cutting sections and, therefore, on the different indexable inserts. This can be taken into account in the extended model (Fig. 8).

The tool profile is divided into several cutting sections. The individual indexable inserts successively penetrate the workpiece body and, therefore, it is possible to calculate the formation of non-deformed chip geometries for each indexable insert. In order to define the cutting sections the position with its upper and lower geometrical limitations needs to be known. The position of each cutting section along the tool circumference can be described by the angle  $\delta_{\phi}$ . By this parameter also different angular position of the cutting sections can be considered.

For a better understanding of the tool concept, a hobbing process with an indexable insert tool typically used in the wind power industry is considered. The

tool has a tip diameter of  $d_{a,0} = 300$  mm (Fig. 9). The tool profile is represented by six cutting sections. The division of the cutting sections is symmetrical to the profile center line. The tip area of the tool profile is represented by one left and one right tip indexable insert, as well as by one left and one right indexable insert at the flank. In the lower area of the profile, straight-sided indexable inserts are located. The combination of one right and one left tip indexable insert results in an effective number of tip cutting edges  $Z_{eff}$ . Therefore the flank's indexable inserts are not considered in the definition of the effective tip cutting edges. The cutting loads in the flank area are significantly lower than at the tooth tip. The tool has in total 8.5 groups of indexable inserts along the tool circumference, therefore,  $Z_{eff} = 17$  effective tip cutting edges. The tool profile contains a protuberance that creates a clearance in the tooth root area.

The test gear is a planetary gear with a module of  $m_n = 16$  mm; a pressure angle of  $\alpha_n = 20^\circ$ ; a helix angle of  $\beta = 7.5^\circ$ ; and a tip diameter of  $d_{a,2} = 615$  mm. The gear is made of the steel alloy 18CrNiMo7-6 and has  $z = 35$  teeth and, therefore, for this gear size both hobbing and form milling processes are efficiently used.

With the geometry data from the tool and the workpiece as well as process parameters like axial feed rate, the model calculates the non-deformed geometry

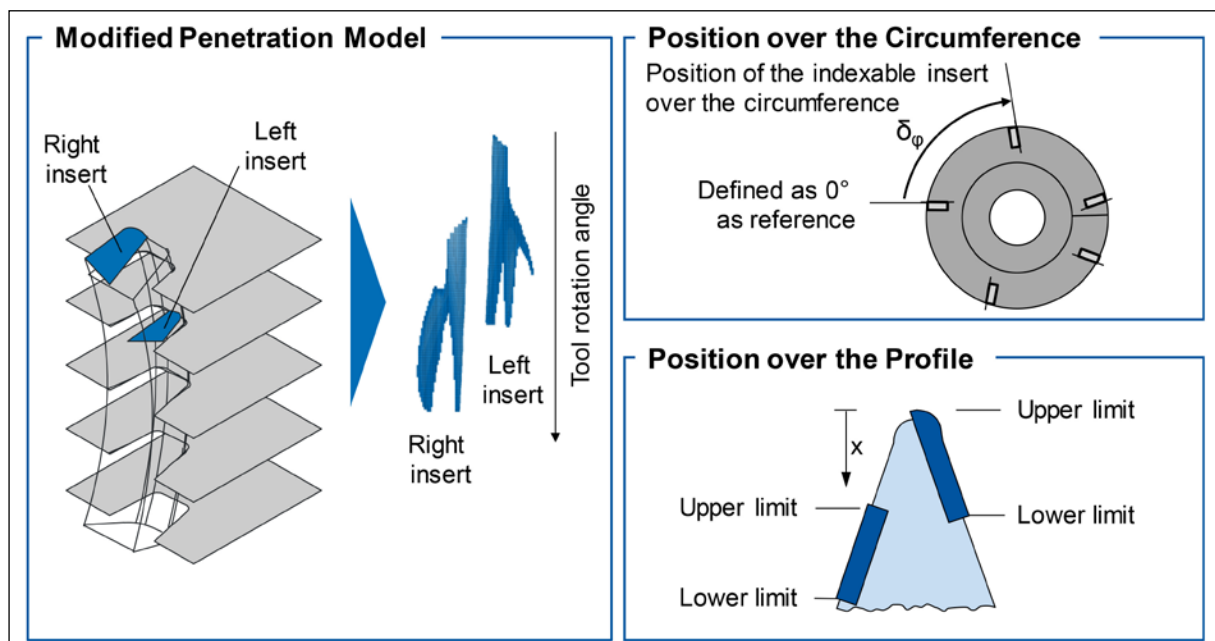


Figure 8: Further development of penetration calculation for application of indexable inserts.

of the intermittent chips. Through the evaluation of the chip geometry, different characteristic values, such as intermittent loads during the process, can be calculated. Currently, the model is able to provide the maximum  $h_{cu,max}$  and average chip thickness  $h_{cu,mit}$ , the related chip volume  $V$  and the maximum and average cutting length,  $l_{max}$  and  $l_{mit}$ , during the process. These characteristic values are output parameters for the entire process as well as individually for each indexable insert over the unrolled tool profile. Hence, the loads at each point of the cutting edge can be determined and evaluated. For the process described above, examples of maximum chip thickness  $h_{cu,max}$ , maximum cutting length  $l_{max}$  and

related volume  $V$  for individual indexable insert over the unrolled tool profile are presented in Figure 10. The course of the maximum chip thickness is divided onto the different indexable inserts. The lower flank indexable inserts Nos. 3 and 6 cut the material with a maximum chip thickness of  $h_{cu,max}=0.14$  mm. The course of the upper flank indexable inserts Nos. 1 and 4 can be divided into two sections. The first section has a linear increase that occurs during the flank machining; the second section has a parabolic increase that occurs during the tip machining. The maximum chip thickness is obtained at the upper flank indexable inserts in the tip area of the tool with a value of  $h_{cu,max}=0.34$  mm. The tip indexable insert

Nos. 2 and 5 cut exclusively in the tip area of the tool. The progress of the maximum chip thickness is similar to that of the upper flank indexable inserts in the tip area. The parabolic profile increases to a maximum value of  $h_{cu,max}=0.34$  mm. With the additional application of the tip indexable inserts, the loads in the tip area are distributed over the upper flank and tip indexable inserts. The indexable inserts allocated in the tip area of the tool are evenly distributed over the tool circumference. Because of this, uniform distribution and the same value for the maximum chip thickness of  $h_{cu,max}=0.34$  mm can be found at all tip indexable inserts.

*Method of the calculation of the*

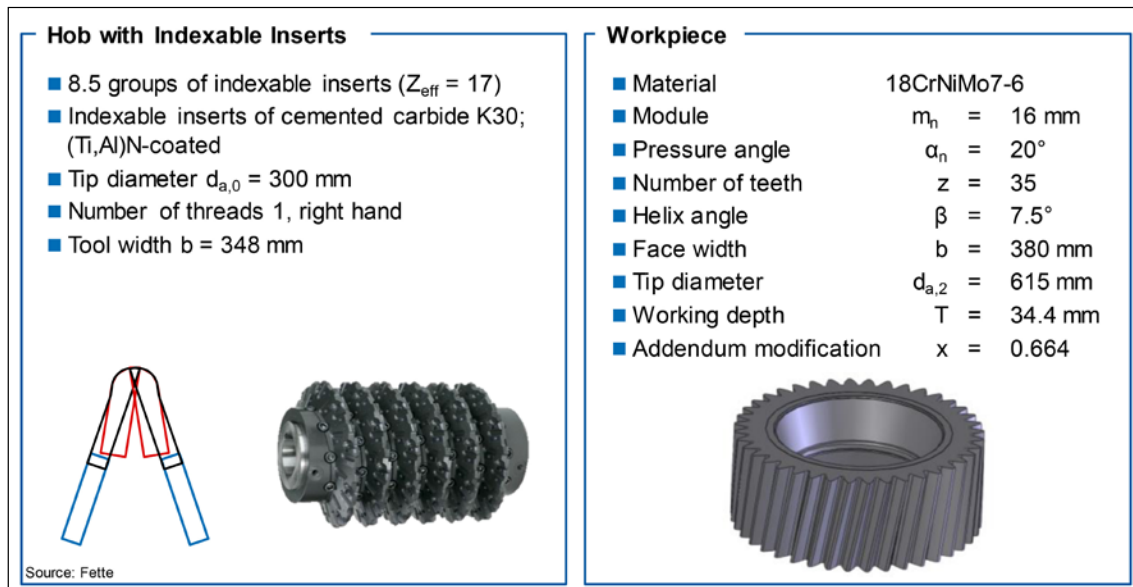


Figure 9 Tool and gear parameters for indexable insert hobbing.

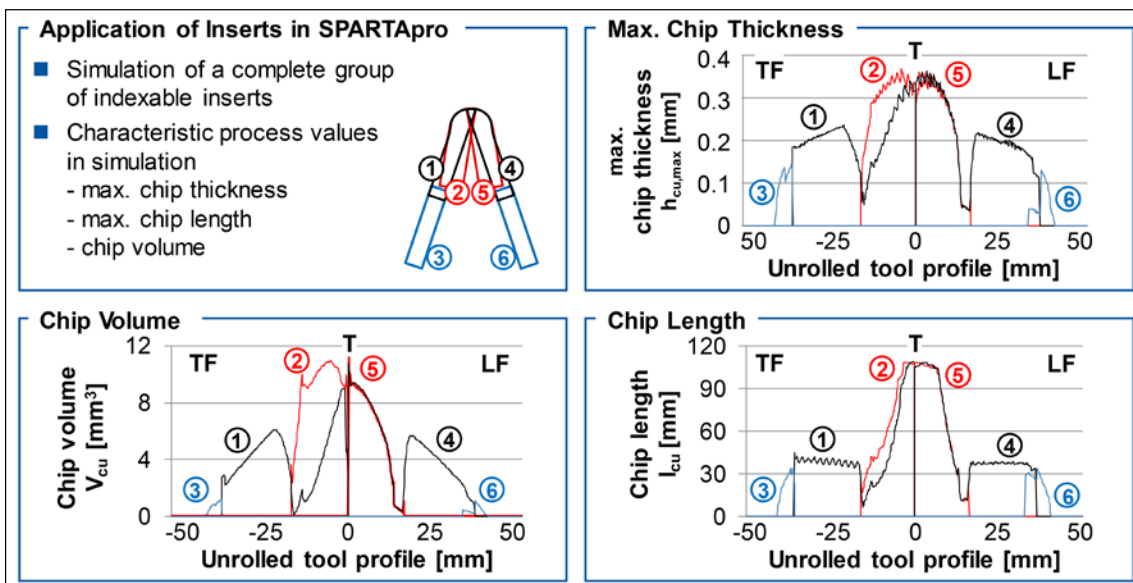


Figure 10 Calculated characteristics values.

**working angles.** The working angles occurring during the process through the variable velocity components along the cutting edge and the rotation angles of the hob can only be reasonably calculated by means of computer support. *SPARTApro* was further developed in order to calculate the working angles along the cutting edge. In the software, the cutting edge is defined by individual points and the number of these points is specified in the *SPARTApro* interface. For each point at the cutting edge, the resultant velocity vector  $V$ , the normal vector  $N$  and the clearance normal vector  $KN$  are calculated (Fig. 11). The velocity vector gives the information regarding the direction of the motion of the point. The normal vector is localized perpendicular to the cutting edge, in the plane of the rake surface. The clearance normal vector is perpendicular to the clearance surface. From the cross product of the normal vector and the clearance normal vector, the  $Pne$  plane is calculated. The  $Pne$  plane is the plane where the working clearance angle is measured. The vector  $Pne$  is perpendicular to the  $Pne$  plane, in the direction of the cutting edge. The cross product between  $Pne$  vector and velocity vector generates a plane called  $Pse$ . The  $Pse$  plane is tangential to the cutting edge, in the direction of the resultant velocity. With the cross product between  $Pse$  vector, the vector perpendicular to the  $Pse$  plane, and the clearance normal vector, the  $A\alpha$  plane is generated. The plane  $A\alpha$  and the clearance surface

are localized in the same plane. The working clearance angle  $\varphi_{fw}$  is the angle measured between the  $Pse$  and the  $A\alpha$  plane in the  $Pne$  plane.

### Analysis of the Working Tool Angle in Machining

The following section about the analysis of working angles during machining includes the description of these angles for each individual test point. The simulation with the software *SPARTApro* (Refs. 14–15) gives an estimation of the influence of the working angles on tool wear behavior. In addition, also presented is the scheduled simulation plan for further KL500/134-1 project developments.

**Design of experiments.** In order to investigate the influence of the working angles on the tool wear during hobbing, the simulation plan is shown (Fig. 12). The adjustment of the tool angles is performed through the relative velocity, shown in Equation 4 and the designed tool angles; the latter can be held in the tool. In order to cover a wide range of parameters it is necessary to vary the designed tool angles. At the starting point of the experimental plan the flank rake angle is  $\sigma_f=0^\circ$ , the clearance angle of  $\varphi_f=6^\circ$  and a maximal chip thickness of  $h_{cu,max}=0.25$  mm. The values established in the experimental plan correspond to the current state of the art. From the base point the designed flank clearance angle  $\varphi_f$  is varied to  $2^\circ$ ,  $10^\circ$  and  $15^\circ$ . The designed flank rake angle is varied in the range of  $-15^\circ$ ,  $-5^\circ$ ,

$0^\circ$ ,  $5^\circ$ ,  $15^\circ$ . The chip thickness plays a decisive role on the wear behavior of the hob (Refs. 16–18) and, therefore, a variation of the chip thickness is taken into consideration in the experimental plan. The values extend from the base point ( $h_{cu,max}=0.25$  mm) upwards to a maximum of  $h_{cu,max}=0.35$  mm and downwards to a minimum of  $h_{cu,max}=0.15$  mm. The gear considered for this experimental plan is a large gear with a module of  $m_n=10$  mm, number of teeth  $z=53$ , helix angle  $\beta=10^\circ$  and a pressure angle of  $\alpha=20^\circ$ .

In order to characterize the tests variants, characteristic values such as maximum chip thickness  $h_{cu,max}$ , average chip thickness  $h_{cu,avg}$ , number of cuts and chip length are calculated with *SPARTApro*. These characteristic values are presented (Fig. 13) as a function of the unrolled tool profile. The curves of the maximum chip thickness have a peak beginning on the tip left flank of the tool. The maximum values are detected in the tip area of the blade for the respective values  $h_{cu,max}=0.15$  mm,  $h_{cu,max}=0.25$  mm and  $h_{cu,max}=0.35$  mm. In the right flank, the curve also drops from tip to root. In the curve for maximum chip thickness, the values of the left flank are smaller than the values of the right flank. It is expected that the variant with the maximum chip thickness of  $h_{cu,max}=0.35$  mm generates the most wear. The cutting forces increase with the increase of the chip thickness, inducing higher loads at the cutting edge.

The curves of the number of cuts

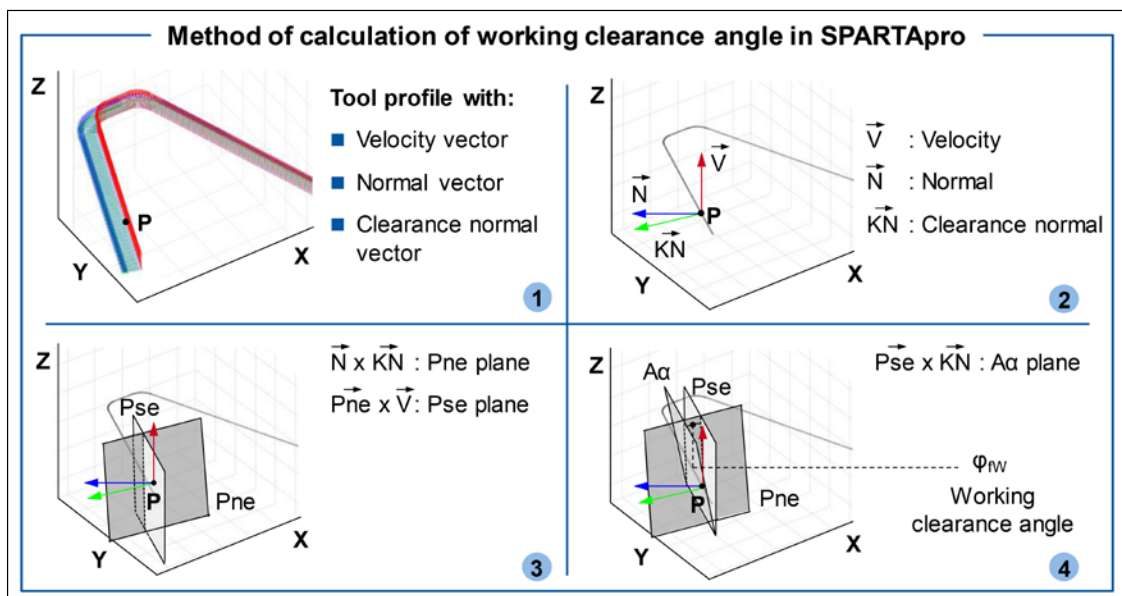


Figure 11 Calculation method of the working clearance angle in *SPARTApro*.

rise on the flank towards the tip. The maximum values are found in the transition area between the left flank and the tip, reaching the value of 27 cuts. In the tip area, the curves drop again, reaching values from 12 to 15 cuts. In the transition area between tip and right flank, the curves rise again.

**Analysis of the working clearance angles.** According to the experimental plan presented, the clearance angle is varied between the values  $\varphi_j=2^\circ, 6^\circ, 10^\circ$  and  $15^\circ$ . The designed clearance angle and the maximum working clearance angle calculated by the simulation are shown (Fig. 14). The clearance angle calculated for each case is plotted over

the unrolled tool profile. The process parameters remain the same for all cases, such as a cutting velocity of  $v_c=120$  m/min, a maximum chip thickness of  $h_{cu,max}=0.25$  mm and designed tip rake angle of  $\sigma_a=0^\circ$ . In Figure 14 the designed clearance angle is represented by a dashed line while the working clearance angle is designated by a solid line. For the case with a designed clearance angle of  $\varphi_j=2^\circ$  the working clearance angle on the left flank reaches the value  $\varphi_{fv}=-3^\circ$ . In the tip area the curve for the working clearance angle reaches its maximum, which is identical to the designed clearance angle  $\varphi_j=\varphi_{fv}=20^\circ$ . In the right flank the working clearance angle is established

in  $\varphi_{fv}=7^\circ$ . Thus, the maximum working clearance angle alteration for both left and right flank is the same — only in different directions. The negative value of the working clearance angle on the left flank causes the contact between the left clearance surface and the workpiece tooth flank surface. The resulting mechanical and thermal stresses generated in the tool clearance surface cause an increase of the tool wear.

The curves for the working clearance angle variation of  $\varphi_j=6^\circ, 10^\circ$  and  $15^\circ$  are similar to the variation of the  $\varphi_j=2^\circ$ , but with a shift upwards according to the respective angle variation amount. The case of  $\varphi_j=6^\circ$  shows a working clearance

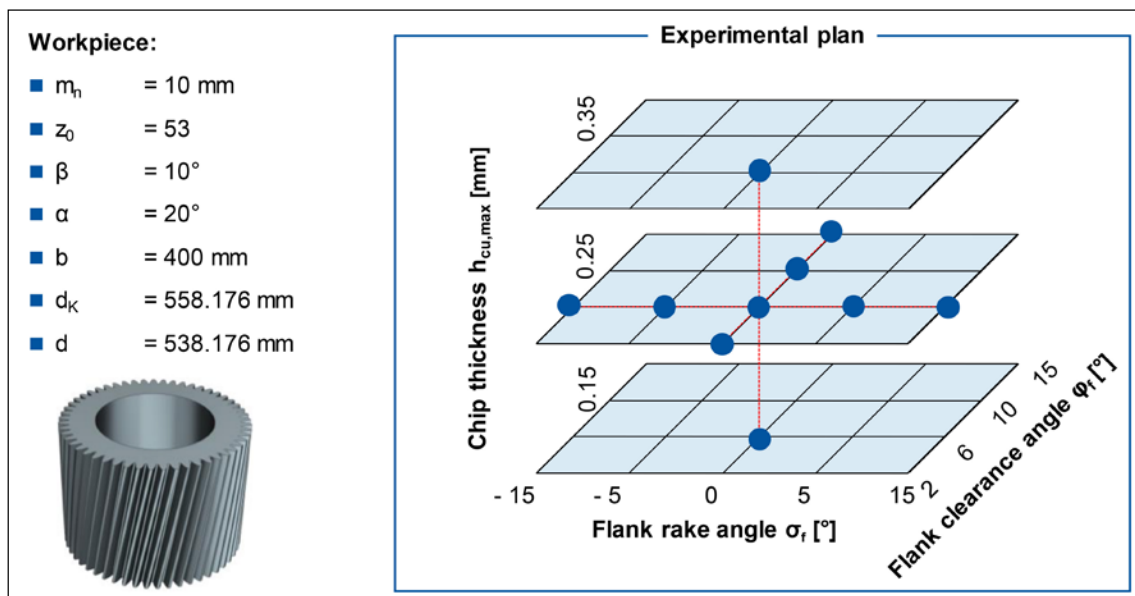


Figure 12 Workpiece and design of experiments.

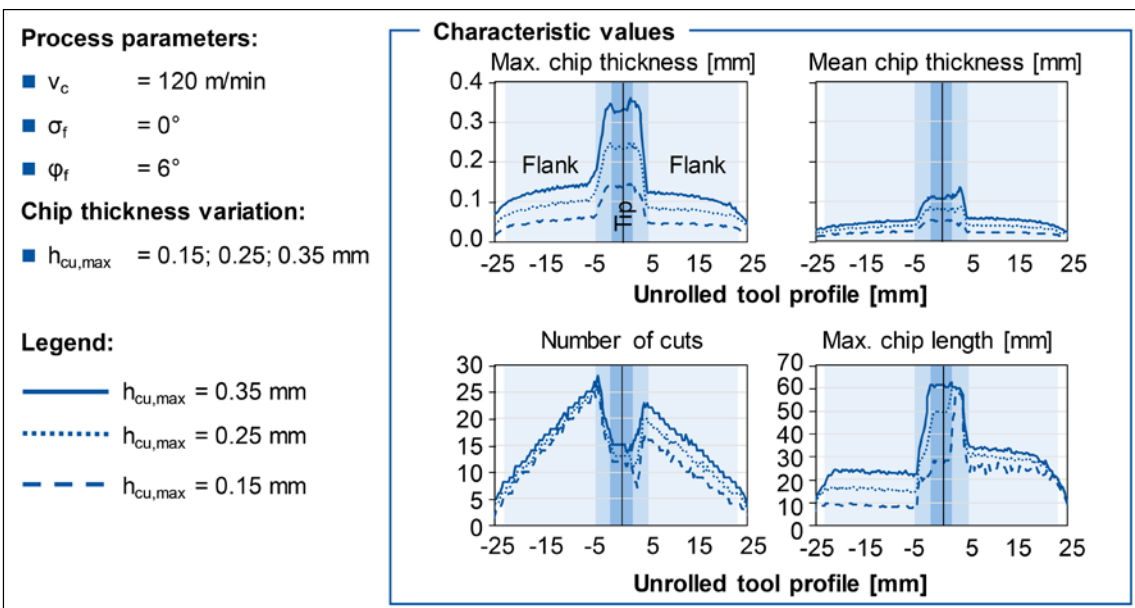


Figure 13 Calculated characteristic values with SPARTApro.

angle of  $\varphi_{fw}=1^\circ$  on the left flank. A small clearance angle leads to a larger contact area and, therefore, an increase the heat flow to the tool substrate. The increase of temperature in the cutting process causes a progressive increase of wear (Ref. 3).

**Analysis of the working rake angles.** Figure 15 shows the designed and working rake angles for each case presented in the experimental plan for the rake angles. As already established in early diagrams, the designed rake angle is represented by a dashed line, while the working rake angle is a solid line. The process parameters used for the tests are the same used in the tests with the clearance angle. The designed rake angles vary between the

values  $\sigma_f=-15^\circ, -5^\circ, 5^\circ$  and  $15^\circ$ . For all four variants, the designed flank clearance angle is established with  $\varphi_f=6^\circ$  and the designed tip rake angle with  $\sigma_a=0^\circ$ . During the cutting process, the tool rake angles of the left flank are different from the rake angles of the right flank. The magnitude of the angles in both flanks are the same, but with an opposite sign. This characteristic is shown in the curve of the designed rake flank angle in Figure 15. For the variant  $\sigma_f=-15^\circ$ , a minimum working flank rake angle of  $\sigma_{fw}=-19^\circ$  is established on the left flank during the process. The large negative rake angles lead to a skive during the cutting process. In addition, the cutting forces will increase and the

following chip will be in contact with the rake surface, causing friction. Due to the large wedge angle of  $\beta=99^\circ$ , the cutting edge is strengthened.

The working rake angle in the tip area of the tool is  $\sigma_{fw}=0^\circ$ . In the transition areas between left flank and tip and between tip and right flank the working flank rake angle increases. The right flank exhibits a maximum working flank rake angle of  $\sigma_{fw}=22^\circ$ , which decreases the cutting forces. In this case, the cutting is sharper and the chip can flow away better from the tool. However, in the same time the wedge angle is reduced to  $\beta=69^\circ$ . Small wedge angles decrease the tool stability and can cause cutting edge breakage.

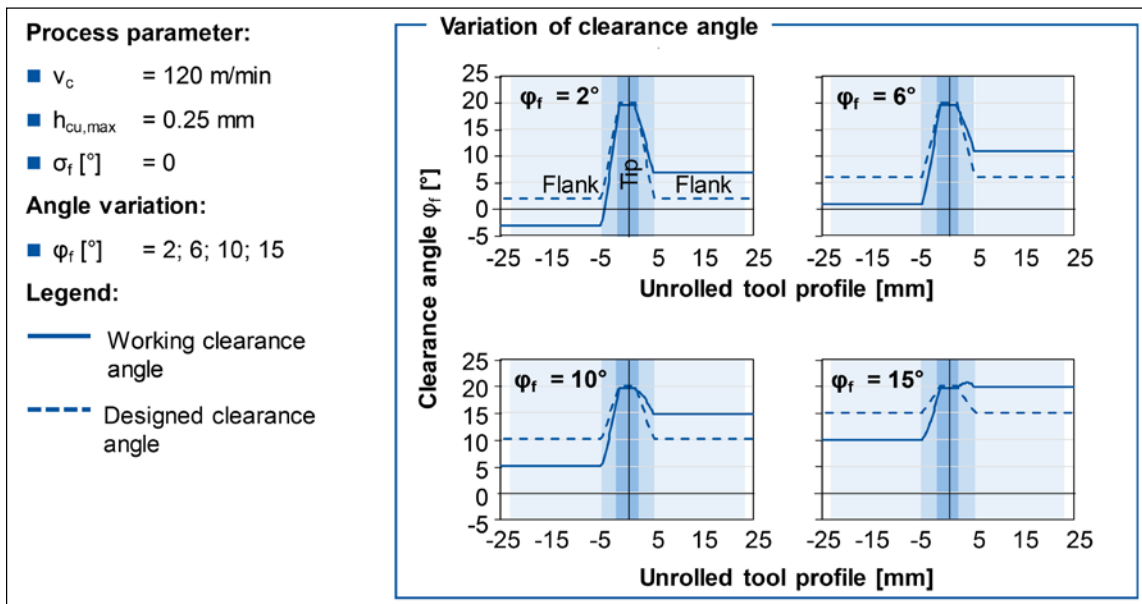


Figure 14 Calculated working clearance angle.

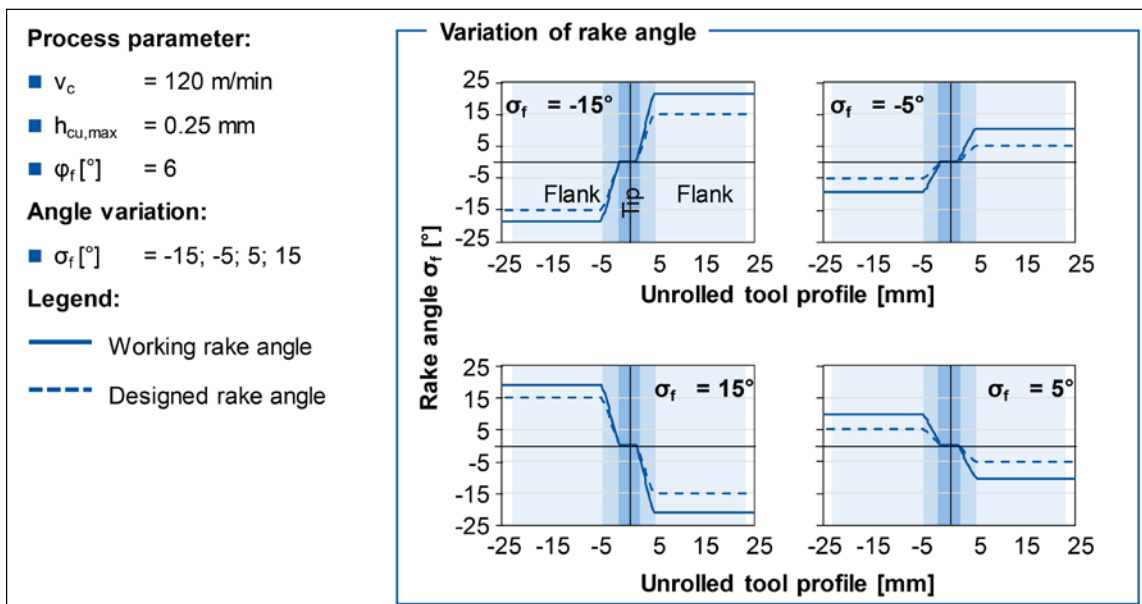


Figure 15 Calculated working rake angle.

For the case where  $\sigma_f = -5^\circ$ , the maximum working rake angle on the left flank is  $\sigma_{fw} = -10^\circ$  and on the right flank the same angle is  $\sigma_{fw} = 10^\circ$ . In order to be able to analyze the effect of the angle on both leading and trailing flank of the tool, the working rake angle is mirrored in the center of the tooth tip, as shown in the diagrams of  $\sigma_f = 5^\circ$  and  $15^\circ$ .

### Summary and Outlook

In this report the working tool angles for an ideal cutting edge and a hob cutting edge were described and analyzed. For optimized hob design, the influence on the tool wear by means of working tool angles is important. Due to the variation of the velocity at the cutting edge and the tool rotation, the working tool angles can be determined only by computer-based calculations. For this purpose *SPARTApro* was further developed, now including a method that can calculate the working tool angles along the cutting edge. A test model was designed for the case of a large gear with a module of  $m_n = 10$  mm. For the test model, an experimental setup was defined, in which the designed rake and clearance angles as well as the chip thickness were varied. The working tool angles were calculated for each point in the experimental setup and an estimation of the influence on the tool wear was given. As the design of tool angles has the highest degree of freedom for hobs with indexable inserts, *SPARTApro* furthermore was enhanced by a method for consideration of split tool profiles with overlap sections.

For further steps experimental tool wear investigations based on the test model are planned. Tools with the angles from the experimental setup will be used, and wear measurements will be performed in constant intervals. From these tests the influence of the working tool angles on the tool wear can be determined more precisely. The developed calculation method can be applied in the wear tests and can give a better understanding for wear phenomena.

**Acknowledgement.** The authors gratefully acknowledge financial support by the German Research Foundation (DFG) [KL 500/134-1] for the achievement of the project results. The authors gratefully acknowledge financial support by the WZL Gear Research Circle for the achievement of the project results

with regards to the enhancement of *SPARTApro*. 

### References

1. Pfauter, H. Pfauter-Wälzfräsen, Berlin, Springer, 1976.
2. Abler, J., K. Felten, C. Kobialka, T. Lierse, A. Mundt, J. Pomp and G. Sulzer. *Verzahnstechnik. Informationen für die Praxis*, Kempten, Druckerei Diet, 2003.
3. Bausch, T. *Innovative Zahnradfertigung. Verfahren, Maschinen und Werkzeuge zur kostengünstigen Herstellung von Stirnrädern mit hoher Qualität ; mit 72 Tabellen. Vol. 175, 3. Ed. Renningen: Expert, 2006.*
4. Klocke, F. and C. Brecher. *Zahnrad- und Getriebetechnik. Auslegung - Herstellung - Untersuchung - Simulation.1. ed. München: Carl Hanser, 2017.*
5. Joppa, K. *Leistungssteigerung beim Wälzfräsen mit Schnellarbeitsstahl durch Analyse, Beurteilung und Beeinflussung des Zerspanprozesses. Diss. RWTH Aachen, 1977.*
6. Rütjes, U. *Entwicklung eines Simulationssystems zur Analyse des Kegelradfräsens. Diss. RWTH Aachen, 2010.*
7. Hardjosuwito, A. *Vorhersage des lokalen Werkzeugstandweges und der Werkstückstandmenge beim Kegelradfräsen. Diss. RWTH Aachen, 2013.*
8. DIN85. *Norm DIN 6581 (Oktober 1985) Begriffe der Zerspantechnik. Bezugssysteme und Winkel am Schneidteil des Werkzeuges.*
9. Klocke, F. and W. König. *Fertigungsverfahren 1. Drehen, Fräsen, Bohren. 8. ed. Berlin: Springer, 2008.*
10. Wolff, A. *Wälzfräser für die Trockenbearbeitung - Auslegung und Geometrie bei Hartmetall- und PM-Werkzeugen Trockene Zahnradvorbearbeitung. Aachen, 13. Oktober 2004, 2004.*
11. Zachmann, K. *Aktueller Einsatz des HSS-Stollenwälzfräasers und HM-Schälwälzfräasers. In: Moderne Zahnradfertigung; Kontakt und Studium Band 175, Vol. 1994, 1994.*
12. Weck, M., W. Winter, F. Klocke and O. Winkel. "Analysis of Gear Hobbing Processes by Manufacturing Simulation," *Production Engineering: Research and Development*, Vol. 2003, 2003, No. Volume X, Issue 1.
13. Brecher, C., M. Brumm and M. Krömer. "Design of Gear Hobbing Processes Using Simulations and Empirical Data," *9th CIRP Conference on Intelligent Computation in Manufacturing Engineering*, Neapel, 23. - 24.06.2014, 2014.
14. Klocke, F., C. Brecher, C. Löpenhaus and M. Krömer. "Influence of Tolerances on Characteristic Manufacturing Deviations in Soft Gear Machining," *International Conference on Gears 2015*. 2015, 2015.
15. Mundt, A. "Modell zur rechnerischen standzeitbestimmung beim Wälzfräsen," *Diss. RWTH Aachen, 1992.*
16. Winkel, O. *Steigerung der Leistungsfähigkeit von Hartmetallwälzfräsern durch eine optimierte Werkzeuggestaltung, Diss. RWTH Aachen, 2005.*
17. Hipke, M. "Wälzfräsen mit pulvermetallurgisch hergestelltem Schnellarbeitsstahl," *Diss. TU Magdeburg, 2012 WZL Gear Conference in the USA 8-20.*

**Felix Kühn M. Sc.** studied mechanical engineering at RWTH Aachen University. In 2015, he started as a research assistant at the chair of Manufacturing Technologies at the Laboratory for Machine Tools (WZL) at RWTH Aachen University for Prof. F. Klocke. Kühn's research is focused upon tool optimization for gear hobbing and roughness analysis of the hobbled tooth root.



**Dr.-Ing. Dipl.-Wirt.-Ing. Christoph Löpenhaus** has since 2014 served as Chief Engineer in the Gear Department of WZL, RWTH Aachen/Laboratory of Machine Tools and Production Engineering (WZL), RWTH Aachen. He previously held positions there as (2011–2014) Team Leader, Group Gear Testing Gear Department Chair of Machine Tools Laboratory of Machine Tools and Production Engineering (WZL) RWTH Aachen; (2010–2011) Research Assistant, Group Gear Testing Gear Department Chair of Machine Tools Laboratory of Machine Tools and Production Engineering (WZL) RWTH Aachen; (2007–2009) as Student Researcher, Group Gear Design and Manufacturing Calculation Gear Department Chair of Machine Tools Laboratory of Machine Tools and Production Engineering (WZL) RWTH Aachen; and (2004–2009) as a student in Industrial Engineering RWTH Aachen.



**Prof. Dr.-Ing. Dr.-Ing. E.h. Dr. h.c. Dr. h.c. Fritz Klocke** began his distinguished career (1970–1973) as an apprenticed toolmaker while at the same time pursuing his production engineering studies at Lemgo/Lippe Polytechnic, and later (1973–1976) at Technical University Berlin. He then (1977–1981) went on to serve as Assistant at the Institute for Machine Tools and Production Engineering, Technical University Berlin. Starting in 1981, Klocke achieved or received the following academic credentials and awards: Chief Engineer; (1982) Doctorate in engineering; (1984–1994) employed at Ernst Winter & Sohn GmbH & Co., Norderstedt; (1984) Head of Process Monitoring; (1985) Technical Director, Mechanical Engineering Department; (1985) Awarded Otto Kienzle Medal by the Universities Production Engineering Group; (1995) Director of the Chair of Manufacturing Technology at the Institute for Machine Tools and Production Engineering (WZL) of the RWTH Aachen, and director of the Fraunhofer Institute for Production Technology, Aachen; (2001–2002) Dean of the Faculty for Mechanical Engineering; (2006) Honorary Ph.D. by the University of Hannover; (2007–2008) President of the International Academy for Production Engineering (CIRP); (2009) Honorary Ph.D. by the University of Thessaloniki; (2010) Honorary Ph.D. by the Keio University; Award of Fraunhofer Medal; (2012) Fellow of the Society of Manufacturing Engineers (SME); (2014) Eli Whitney Productivity Award (SME); and (2014) Fellow of RWTH Aachen University.



For Related Articles Search

**hobbing** 

at [www.geartechnology.com](http://www.geartechnology.com)